Control Engineering Practice 138 (2023) 105608

Contents lists available at ScienceDirect

Control Engineering Practice

journal homepage: www.elsevier.com/locate/conengprac

A robust adaptive formation control methodology for networked multi-UAV systems with applications to cooperative payload transportation

Yu-Hsiang Su [a], Parijat Bhowmick [b,*], Alexander Lanzon [a]

[a] Department of Electrical and Electronic Engineering, School of Engineering, University of Manchester, Manchester M13 9PL, UK
[b] Department of Electronics and Electrical Engineering, IIT Guwahati, North Guwahati, Assam 781039, India

ARTICLE INFO

Keywords:
Adaptive formation control
Multi-agent systems
Cooperative payload transportation
UAVs
Lyapunov stability

ABSTRACT

This paper develops a new robust adaptive formation control methodology for networked multi-UAV systems to solve the cooperative payload transportation problem. This methodology offers a simple yet effective technique for object transportation relying on the formation tracking principle in the presence of bounded exogenous disturbances. Compared to existing techniques, the proposed method resorts to the σ-modification approach to resolve the parameter drift phenomenon. The ultimate boundedness of the formation tracking error dynamics is established by utilising Lyapunov theory. In addition, the proposed scheme does not involve any multi-body dynamics problem, nor does it require any reference model, disturbance filter/estimator or any prior knowledge of the disturbances. As a result, it reduces the overall complexity of the formation control scheme. The paper includes extensive simulation case studies accompanied by lab-based experimental validation results conducted on a group of nano quadcopter UAVs to demonstrate the feasibility and performance of the controller. The paper also projects a potential application of the proposed scheme in cooperative payload transportation missions.

1. Introduction

During the last fifteen years, the payload transportation problem by UAVs has gained significant research interest from the robotics and control communities. It has widespread real-world applications (see Maza, Kondak, Bernard, and Ollero (2010), Michael, Fink, and Kumar (2011) and Villa, Brandao, and Sarcinelli-Filho (2019) and references therein), such as in industrial automation, doorstep product delivery (Amazon, 2016), construction automation (Lindsey, Mellinger, & Kumar, 2012), transporting relief materials to flood-affected or earthquake-devastated areas, space/deep sea exploration, etc. However, using a single UAV for payload transportation missions comes with several drawbacks, including limited payload capacity, limited flying time, operational failures caused by UAV malfunctions, etc. To overcome these problems, a promising solution is to incorporate multiple UAVs to carry out payload transportation missions. Compared to a single UAV, transporting objects using a team of networked UAVs offers several advantages, such as significantly increased payload-carrying capacity, enhanced safety and reliability, smoother operation, fault tolerance to UAV malfunctions, longer operation time, optimal battery-power utilisation, etc.

Significant research has already been done on cooperative payload transportation problems (by means of multiple UAVs) considering different practical constraints. Some methodologies focused on precise trajectory control of the suspended payload and motion planning for each UAV via a centralised method. For example, Michael et al. (2011) recommended particular UAV configurations to ensure a static equilibrium of the payload and used an optimisation algorithm to generate the trajectories for each UAV such that the suspended payload can track the desired pose. A geometric control scheme was proposed in Lee (2018) for a multi-UAV system, which facilitates suspended payloads to follow the desired position and attitude trajectories. Tartaglione, D'Amato, Ariola, Rossi, and Johansen (2017) developed an MPC-based trajectory tracking control scheme and obstacle avoidance technique such that a fleet of UAVs can safely accomplish a cooperative transportation mission. The other approaches build on the collaborative movement of a group of stable UAVs while carrying a suspended payload attached to them. For instance, Mohammadi, Sirouspour, and Grivani (2020) proposed a passivity-based cooperative control scheme for a multi-UAV system with an inner-loop PID controller to facilitate object transportation. This methodology involves a time-varying energy dissipative term to ensure closed-loop asymptotic stability when the UAVs carry a suspended payload. Marina and Smeur (2019) combined a distance-based formation control scheme and an Incremental Nonlinear Dynamic Inversion control strategy to achieve collaborative payload transportation by a group of UAVs. In Klausen, Meissen, Fossen, Arcak, and Johansen (2020), a decentralised formation control scheme depending on an internal feedback control strategy was proposed for a

* Corresponding author.
E-mail address: parijat.bhowmick@iitg.ac.in (P. Bhowmick).

https://doi.org/10.1016/j.conengprac.2023.105608
Received 24 December 2022; Received in revised form 28 May 2023; Accepted 19 June 2023
Available online xxxx
0967-0661/

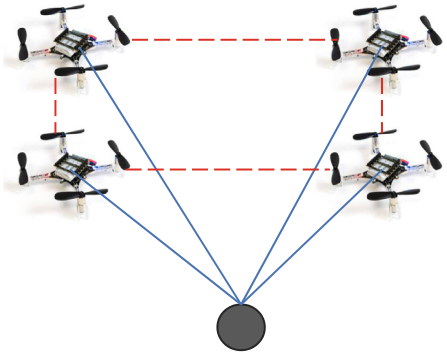

Fig. 1. An illustration of a cooperative payload transportation mission by networked quadcopter UAVs. The red dashed lines represent the formation of the quadcopter UAVs, while the blue lines represent the cables/strings. (For interpretation of the references to colour in this figure legend, the reader is referred to the web version of this article.)

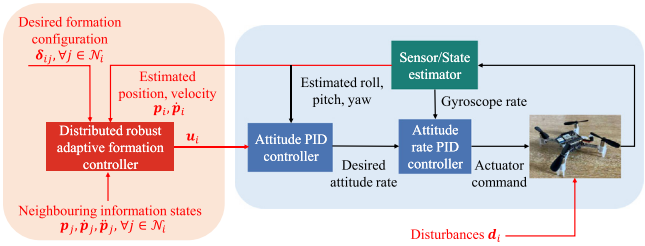

Fig. 2. The proposed two-loop formation control configuration for the real-time flight experiments conducted on a group of networked UAVs.

team of UAVs to transport a suspended payload in the presence of wind disturbances.

Formation control has been a major thrust area in the domain of cooperative control of multi-agent systems (e.g. multi-UAV and multi-robot systems) (Hu, Bhowmick and Lanzon, 2021). It requires networked agents to achieve and maintain a prescribed geometric shape (Ren, Beard, & Atkins, 2007). Various formation control problems for networked UAVs have been addressed in the literature, such as static formation (Hu, Bhowmick, & Lanzon, 2020; Turpin, Michael, & Kumar, 2012), time-varying formation (Dong, Yu, Shi, & Zhong, 2015; Hu & Lanzon, 2018), formation control with switching topologies (Dong, Zhou, Ren, & Zhong, 2016), formation control ensuring collision avoidance (Toksoz, Oguz, & Gazi, 2019), formation in a constrained environment (Wang et al., 2020), etc. However, the literature mentioned earlier does not take into account the effect of exogenous disturbances or uncertainties, such as model uncertainties, communication delays, and data losses. As a result, these formation control schemes may not be robust to external disturbances or uncertainties. Recently, the Model Reference Adaptive Control (MRAC) principle has been utilised to develop advanced formation control methodologies for multi-agent and multi-UAV systems subject to model uncertainties and disturbances, such as in Baldi and Frasca (2019), Cardona, Arevalo-Castiblanco, Tellez-Castro, Calderon, and Mojica-Nava (2021), Dogan, Gruenwald, Yucelen, Muse, and Butcher (2019) and Xuan-Mung and Hong (2019). Liu, Ma, Lewis, and Wan (2020) designed a filter to suppress the effect of disturbances during the formation control of UAVs. Wang, Bi, Wang, Kuang, and Wang (2022) proposed an observer-based event-triggered formation control scheme for networked UAVs with compensation for disturbances. Zhou, Tao, Paszke, Stojanovic, and Yang (2020) used an iterative learning control method to address the uncertainty problem in spatially interconnected systems. Chen, Zhang, Stojanovic, Zhang, and Zhang (2020) dealt with the data missing problem in networked systems by using an event-triggered fuzzy control method.

Motivated by the remarkable progress in cooperative payload transportation through formation control of multi-UAVs, this paper aims to deploy a team of networked UAVs flying in a prescribed formation for transporting a suspended payload attached to them, as illustrated in Fig. 1. As long as the networked UAVs maintain the prescribed formation and synchronise their motion, they can carry a payload to a final destination. The payload is suspended by several cables or strings attached to the UAVs. The tensile forces (or the tension) generated in the strings are modelled as unknown bounded exogenous disturbances acting on the UAVs. This new methodology offers a simple yet effective and easy-to-implement technique for cooperative object transportation. The proposed methodology recommends a two-loop control configuration, shown in Fig. 2, in which the inner loop deploys a cascaded PID controller block to stabilise the attitude dynamics, while the outer loop applies a robust adaptive formation control scheme to the translational dynamics of the UAVs. Compared to existing literature that applied Model Reference Adaptive Control techniques (e.g. Baldi and Frasca (2019), Cardona et al. (2021), Dogan et al. (2019) and Xuan-Mung and Hong (2019)) or used a disturbance filter/estimator (e.g. Liu et al. (2020) and Wang et al. (2022)) to compensate the effect of external disturbances, we exploit the σ-modification approach. The new formation control methodology does not need to solve any multi-body mechanics/dynamics problem, neither it depends on any reference model, prior knowledge of the exogenous disturbances or any disturbance filter/observer. Therefore, it reduces the overall complexity of the formation control scheme. In addition, we have included a real-world quadcopter application in which a team of networked UAVs has successfully accomplished a cooperative payload transportation flight mission under the influence of the proposed formation control scheme. The salient features and key contributions of this research work are mentioned below:

1. This paper proposes a *new* robust adaptive formation control methodology for networked UAVs subject to bounded exogenous disturbances. We exploit the σ-modification approach instead of using well-known Model Reference Adaptive Control (MRAC) techniques to deal with the unknown disturbances in the formation control problem of multi-agent systems;
2. The performance of the proposed formation control scheme has been tested against that of a recent article (Hu, Bhowmick, Jang, Arvin and Lanzon, 2021) via Matlab simulations. The results reveal that the proposed formation scheme, which considers the effect of disturbances, efficiently addresses the *parameter drift phenomenon*. To the best of our knowledge, this is the first paper to investigate the issue of the parameter drift phenomenon in the adaptive formation control problem of multi-agent systems and to resolve the problem using the σ-modification technique;
3. The proposed methodology relies on the formation tracking principle to address the cooperative payload transportation problem, providing a simple yet effective solution without requiring reference models, disturbance filters/estimators, or prior knowledge of disturbances. Furthermore, we utilise the proposed formation control scheme to carry out a cooperative payload transportation flight mission using a group of networked UAVs, demonstrating its usefulness in real-world applications. Compared with existing works based on a centralised method (Lee, 2018; Michael et al., 2011; Tartaglione et al., 2017), our method can be easily implemented on UAVs and allows for scalability due to its distributed nature;
4. We have provided lab-based experimental validation results performed on a group of Crazyflie 2.1 nano quadcopter UAVs to demonstrate the feasibility and performance of the proposed scheme, in contrast to many existing works (e.g. Baldi and Frasca (2019), Cardona et al. (2021), Dogan et al. (2019), Liu et al. (2020) and Xuan-Mung and Hong (2019)) that contain only simulation results.

The rest of the paper is organised as follows: Section 2 provides important preliminaries and describes the problem statement. Section 3 presents the primary result of this paper, which develops a robust adaptive formation control methodology for networked UAVs subject to unknown bounded exogenous disturbances. Section 4 compares the robustness of the proposed formation controller with a benchmark adaptive formation controller via Matlab simulations. Section 5 presents the results of the real-time flight experiments in which we demonstrate a cooperative payload transportation flight mission using four networked Crazyflie nano quadcopter UAVs. Finally, Section 6 concludes the paper.

The notations and acronyms are standard throughout. $\mathbb{R}$ denotes the set of all real numbers; while $\mathbb{R}_{\geq 0}$ and $\mathbb{R}_{>0}$ denote respectively the sets of all non-negative and positive real numbers. Let $\mathbf{1}_n$ be the column vector with all n entries equal to 1. $\|.\|$ is used to represent the 2-norm of a vector or a matrix. The Kronecker product of two matrices A and B is denoted by $A \otimes B$.

2. Technical background and problem formulation

We will now introduce important Lemmas which are required in proving our theorem.

Lemma 1 (*Bernstein, 2009, Young's Inequality*). *If x and y are non-negative real numbers and p and q are positive real numbers such that $\frac{1}{p}+\frac{1}{q}=1$, then $xy \leq \frac{x^p}{p}+\frac{y^q}{q}$. The equality condition holds if and only if $x^p = y^q$.*

Lemma 2 (*Ding, 2013, Comparison Lemma (Lemma 4.5)*). *Let $g, V : [0,\infty) \to \mathbb{R}$. Then*

$$\dot{V}(t) \leq -aV(t) + g(t) \qquad \forall t \geq 0$$

implies that

$$V(t) \leq e^{-at}V(0) + \int_0^t e^{-a(t-\tau)}g(\tau)\,d\tau \qquad \forall t \geq 0$$

for any finite constant $a \in \mathbb{R}_{>0}$.

2.1. Interaction topology

A team of networked UAV agents exchanges information among themselves according to an interaction topology. In this paper, we use a weighted directed graph $\mathcal{G} = \{\mathcal{V}, \mathcal{E}, \mathcal{A}\}$ to represent the interaction topology between each pair of UAV agents. Here, $\mathcal{V} = \{v_1, \ldots, v_N\}$ is the node set, $\mathcal{E} \subset \mathcal{V} \times \mathcal{V}$ is the edge set and $\mathcal{A} = [a_{ij}] \in \mathbb{R}^{N\times N}$ is the associated adjacency matrix respectively. The edge $e_{ji} = (v_j, v_i) \in \mathcal{E}$ denotes the information passes from node j to node i, which means that node j is a neighbour of node i. In addition, we define the set of all neighbours of node i as $\mathcal{N}_i = \{v_j | (v_j, v_i) \in \mathcal{E}\}$. a_{ij} represents the weight of e_{ji}. The adjacency matrix $\mathcal{A}$ is defined as $a_{ii} = 0$, $a_{ij} > 0$ if $e_{ji} \in \mathcal{E}$ and $a_{ij} = 0$ otherwise. The Laplacian matrix $\mathcal{L} = [l_{ij}] \in \mathbb{R}^{N\times N}$ associated with $\mathcal{G}$ is defined by $l_{ii} = \sum_{j\neq i} a_{ij}$ and $l_{ij} = -a_{ij}$ when $i \neq j$. A directed graph is said to have a directed spanning tree if the graph has at least one node (called the *root node*) with directed paths to every other node.

2.2. Modelling of the quadcopter UAVs

The dynamics of small and lightweight quadcopter UAVs, such as Crazyflie nano quadcopters (Bitcraze, 0000), can be represented by the following Newton–Euler equations:

$$\begin{cases} m\ddot{\mathbf{p}} = -mg\mathbf{e}_z + \mathbf{R}_e^b(\boldsymbol{\eta})\mathbf{F}_b, \\ \mathbf{I}\dot{\boldsymbol{\omega}} = -\boldsymbol{\omega} \times \mathbf{I}\boldsymbol{\omega} + \boldsymbol{\tau}_b, \end{cases} \tag{1}$$

where $\mathbf{p} = [x, y, z]^\top$ and $\boldsymbol{\omega} = [p, q, r]^\top$ are the position vector in the Earth-reference frame and the angular velocity vector in the body-reference frame. $m \in \mathbb{R}$ and $\mathbf{I} \in \mathbb{R}^{3\times 3}$ denote the mass and the inertia matrix of a quadcopter UAV. $\mathbf{F}_b = [0, 0, T]^\top$ and $\boldsymbol{\tau}_b$ signify the total force vector and total drag torque vector acting on a quadcopter UAV in the body-reference frame. T is the total thrust produced by the four rotors. g is the gravity constant and $\mathbf{e}_z = [0, 0, 1]^\top$ is the unit vector in the Earth-reference frame. The rotation matrix for transforming a vector from the body frame to the Earth frame following the $Z \to Y \to X$ rotation sequence is given by

$$\mathbf{R}_e^b(\boldsymbol{\eta}) = \begin{bmatrix} c\theta c\psi & s\phi s\theta c\psi - c\phi s\psi & c\phi s\theta c\psi + s\phi s\psi \\ c\theta s\psi & s\phi s\theta s\psi + c\phi c\psi & c\phi s\theta s\psi - s\phi c\psi \\ -s\theta & s\phi c\theta & c\phi c\theta \end{bmatrix} \tag{2}$$

where $\boldsymbol{\eta} = [\phi, \theta, \psi]^\top$ denote the Euler angles, $c\phi \triangleq \cos\phi$ and $s\phi \triangleq \sin\phi$. The relation between the angular velocity and the derivatives of the Euler angles can be expressed as:

$$\begin{bmatrix} p \\ q \\ r \end{bmatrix} = \begin{bmatrix} 1 & 0 & -\sin\theta \\ 0 & \cos\phi & \sin\phi\cos\theta \\ 0 & -\sin\phi & \cos\phi\cos\theta \end{bmatrix} \begin{bmatrix} \dot{\phi} \\ \dot{\theta} \\ \dot{\psi} \end{bmatrix}. \tag{3}$$

Remark 1. Since the attitude dynamics of a quadcopter UAV are much faster than its translational dynamics, hovering and manoeuvring (i.e. translation) can be controlled together by a two-loop control scheme as shown in Fig. 2 (see Dong et al. (2015, 2016), Guo, Jia, Yu, Guo, and Xie (2020), Kendoul (2009) and Su and Lanzon (2022)). The robust adaptive formation control laws are implemented in the outer loop and govern networked UAVs to achieve the desired formations/positions and synchronise their motions to keep tracking a virtual leader/target. At the same time, the inner loop employs cascade PID controllers to stabilise the attitude dynamics. As a result, the closed-loop translational dynamics of a quadcopter UAV after closing the inner loop can be approximated by a double integrator system $\ddot{\mathbf{p}}_i = \mathbf{u}_i$, where $\mathbf{p}_i = [x_i, y_i, z_i]^\top$ and $\mathbf{u}_i = [u_{x_i}, u_{y_i}, u_{z_i}]^\top$ are the position and the control input vectors of the i^{th} quadcopter UAV. The control input computed from the outer loop can be transformed into the desired thrust (T^d), roll angle (ϕ^d) and pitch angle (θ^d), that is

$$\begin{cases} T_i^d = m\sqrt{u_{x_i}^2 + u_{y_i}^2 + \left(u_{z_i} + g\right)^2}, \\ \phi_i^d = \sin^{-1}\left(m\dfrac{u_{x_i}\sin\psi_i^d - u_{y_i}\cos\psi_i^d}{T}\right), \\ \theta_i^d = \tan^{-1}\left(\dfrac{u_{x_i}\cos\psi_i^d - u_{y_i}\sin\psi_i^d}{u_{z_i} + g}\right), \end{cases} \tag{4}$$

where ψ_i^d is the desired yaw angle to be assigned by the user.

2.3. Problem statement

Consider a team of N networked UAV agents whose closed-loop translational dynamics can be approximated by

$$\begin{cases} \dot{\mathbf{p}}_i = \mathbf{v}_i, \\ \dot{\mathbf{v}}_i = \mathbf{u}_i + \mathbf{d}_i, \end{cases} \qquad \forall i \in \{1, \ldots, N\} \tag{5}$$

where $\mathbf{p}_i \in \mathbb{R}^3$ is the position vector, $\mathbf{v}_i \in \mathbb{R}^3$ is the velocity vector and $\mathbf{u}_i \in \mathbb{R}^3$ is the control input vector of the i^{th} quadcopter and $\mathbf{d}_i \in \mathbb{R}^3$ accounts for the exogenous disturbances. $\|\mathbf{d}_i(t)\| \leq d_0$ $\forall t \geq 0$ where $d_0 \in \mathbb{R}_{>0}$ is a finite upper bound of the disturbance amplitude. In a cooperative payload transportation mission, we use $\mathbf{d}_i$ to capture the tensile force caused by the suspended payload. Hence, it affects the acceleration $\dot{\mathbf{v}}_i$ state-equation. We also consider a virtual leader/target, labelled as the $(N+1)^{\text{th}}$ node, to provide a reference trajectory for the follower UAV agents to track. This virtual leader/target is treated as an exo-system described below, and it is independent of the agent dynamics and the payload:

$$\begin{cases} \dot{\mathbf{p}}_{N+1} = \mathbf{v}_{N+1}, \\ \dot{\mathbf{v}}_{N+1} = \mathbf{a}_{\text{ref}}, \end{cases} \tag{6}$$

where $\mathbf{p}_{N+1} \in \mathbb{R}^3$, $\mathbf{v}_{N+1} \in \mathbb{R}^3$ and $\mathbf{a}_{\text{ref}} \in \mathbb{R}^3$ are respectively the position, velocity and the given acceleration reference vectors. Let $\boldsymbol{\delta}_{ij} \in \mathbb{R}^3$ denote the formation configuration (also known as the formation offset) between the i^{th} and j^{th} quadcopters where $i \in \{1, \dots, N\}$ and $j \in \mathcal{N}_i$. The interaction topology between each quadcopter and the virtual leader/target is described by a directed graph $\mathcal{G} = \{\mathcal{V}, \mathcal{E}, \mathcal{A}\}$. We will now mention an important assumption that must be satisfied for the interaction topology among the agents.

Assumption 1. The communication (or interaction) topology among the agents, denoted by $\mathcal{G}$, contains a directed spanning tree with the virtual leader/target being the root node.

According to Assumption 1, the Laplacian matrix $\mathcal{L}$ corresponding to $\mathcal{G}$ can be partitioned as shown below:

$$\mathcal{L} = \begin{bmatrix} \mathcal{L}_1 & \mathcal{L}_2 \\ 0_{1\times N} & 0_{1\times 1} \end{bmatrix} \tag{7}$$

where $\mathcal{L}_1 \in \mathbb{R}^{N\times N}$ stands for the sub-Laplacian matrix describing the interactions among the UAV agents and $\mathcal{L}_2 \in^{N\times 1}$ is the sub-Laplacian matrix that expresses the relationship among the UAV agents and the virtual leader/target. The following Lemma gives an important technical result of algebraic graph theory, which will be invoked in Section 3 to derive the proof of Lemma 4.

Lemma 3 (*Meng, Ren, & You, 2010, Lemma 4*). *Each entry of $-\mathcal{L}_1^{-1}\mathcal{L}_2$ is non-negative and each row sum of $-\mathcal{L}_1^{-1}\mathcal{L}_2$ is equal to one.*

The primary objectives of this work are as follows:

- To develop a robust adaptive formation control methodology for networked UAV agents to achieve a prescribed formation and synchronise their motions to keep tracking a virtual leader/target in the presence of bounded exogenous disturbances;
- To implement the proposed methodology on a group of networked quadcopter UAVs and successfully perform a cooperative payload transportation mission.

Note that no prior or explicit knowledge about the suspended payload is considered in the control design. Instead, it is treated as bounded exogenous disturbances $\mathbf{d}_i$ in the translational dynamics model of each UAV agent in Eq. (5).

3. A robust adaptive formation control methodology

This section presents the key development of this paper. A robust adaptive formation control methodology is developed for a networked multi-UAV system subject to bounded exogenous disturbances, relying on a σ-modification technique. We will now provide a brief background to introduce the main results.

For each UAV agent, we define the formation error $\boldsymbol{\xi}_i \in \mathbb{R}^3$ w.r.t. its neighbouring agents as

$$\boldsymbol{\xi}_i = \sum_{j\in\mathcal{N}_i} a_{ij}\left(\mathbf{p}_i - \mathbf{p}_j - \boldsymbol{\delta}_{ij}\right) \quad \forall i \in \{1, \dots, N\}, \tag{8}$$

where $\boldsymbol{\delta}_{ij}$ is the formation offset between the i^{th} and j^{th} UAV agents. Similarly, we define the velocity error $\boldsymbol{\zeta}_i \in \mathbb{R}^3$ for each UAV agent w.r.t. its neighbours as

$$\boldsymbol{\zeta}_i = \sum_{j\in\mathcal{N}_i} a_{ij}\left(\mathbf{v}_i - \mathbf{v}_j\right) \quad \forall i \in \{1, \dots, N\}. \tag{9}$$

Definition 1 (*Formation Control*). A multi-agent system (e.g. a team of networked UAVs or robots) is said to attain the desired formation, specified by the formation configuration vector $\mathbf{h}$ w.r.t. the virtual leader/target, if the position of each UAV agent $\mathbf{p}_i(t)$ satisfies the relationship

$$\lim_{t\to\infty} \mathbf{p}_i(t) - \mathbf{p}_j(t) = \boldsymbol{\delta}_{ij} \tag{10}$$

for all $i \in \{1, \dots, N\}$ and $j \in \mathcal{N}_i$, where

$$\boldsymbol{\delta}_{ij} = \mathbf{h}_i - \mathbf{h}_j \qquad \forall j \in \mathcal{N}_i. \tag{11}$$

Lemma 4. *Consider a multi-agent system consisting of N agents connected via a directed graph that satisfies Assumption 1. The agents are said to attain the desired formation, specified by $\mathbf{h}$ and satisfying (11), if and only if*

$$\lim_{t\to\infty}\left(\sum_{j\in\mathcal{N}_i} a_{ij}\left(\mathbf{p}_i(t) - \mathbf{p}_j(t) - \boldsymbol{\delta}_{ij}\right)\right) = \lim_{t\to\infty} \boldsymbol{\xi}_i(t) = 0 \tag{12}$$

for all $i \in \{1, \dots, N\}$.

Proof. According to $\boldsymbol{\delta}_{ij} = \mathbf{h}_i - \mathbf{h}_j$ as mentioned in (11), we can express the formation error $\boldsymbol{\xi}_i$, given in (8), as

$$\boldsymbol{\xi}_i = \sum_{j=1}^{N} a_{ij}\left(\left(\mathbf{p}_i - \mathbf{h}_i\right) - \left(\mathbf{p}_j - \mathbf{h}_j\right)\right) + a_{i,N+1}\left(\left(\mathbf{p}_i - \mathbf{h}_i\right) - \mathbf{p}_{N+1}\right). \tag{13}$$

Note that $\mathbf{h}_i, \mathbf{h}_j \in \mathbb{R}^3$ for all i and j.

Define $\mathbf{z}_i = \mathbf{p}_i - \mathbf{h}_i$, $\mathbf{p} = [\mathbf{p}_1^\top, \mathbf{p}_2^\top, \dots, \mathbf{p}_N^\top]^\top$ and $\mathbf{z} = [\mathbf{z}_1^\top, \mathbf{z}_2^\top, \dots, \mathbf{z}_N^\top]^\top$. Let $\mathbf{h} = [\mathbf{h}_1^\top, \mathbf{h}_2^\top, \dots, \mathbf{h}_N^\top]^\top$ and $\boldsymbol{\xi} = [\boldsymbol{\xi}_1^\top, \boldsymbol{\xi}_2^\top, \dots, \boldsymbol{\xi}_N^\top]^\top$ be respectively the desired formation configuration and formation error vectors. We can express $\boldsymbol{\xi}$ in the Kronecker product form as

$$\boldsymbol{\xi} = \left(\mathcal{L}_1 \otimes I_3\right)\mathbf{z} + \left(\mathcal{L}_2 \otimes I_3\right)\mathbf{p}_{N+1}. \tag{14}$$

Now, if (12) holds, we have $\lim_{t\to\infty} \boldsymbol{\xi}(t) = 0$, which in turn implies from (14)

$$\lim_{t\to\infty}\left[\mathbf{p}(t) - \mathbf{h}(t) + \left(\mathcal{L}_1^{-1}\mathcal{L}_2 \otimes I_3\right)\mathbf{p}_{N+1}(t)\right] = 0. \tag{15}$$

According to Assumption 1 and Lemma 3, we have $\mathcal{L}_1^{-1}\mathcal{L}_2 = -\mathbf{1}_N$. Substituting $\mathcal{L}_1^{-1}\mathcal{L}_2 = -\mathbf{1}_N$ into (15), we get

$$\lim_{t\to\infty}\left[\mathbf{p}(t) - \mathbf{h}(t) - \left(\mathbf{1}_N \otimes I_3\right)\mathbf{p}_{N+1}(t)\right] = 0. \tag{16}$$

From Eq. (16), we conclude that the prescribed formation among the agents also satisfies the condition in (10). This proves that the desired formation is attained if (12) holds. ■

We are now ready to present the main theorem of this paper, which proposes and establishes a new robust adaptive formation control methodology for a team of networked UAVs subject to unknown bounded exogenous disturbances.

Theorem 1. *Consider a team of N homogeneous UAV agents connected via a directed graph $\mathcal{G}$ that satisfies Assumption 1. The closed-loop translational dynamics of each UAV are approximated as double integrator dynamics, as given in Eq. (5). Then the multi-UAV system achieves the desired formation and synchronises its motions to keep tracking a virtual leader or target in the presence of unknown bounded exogenous disturbances $\|\mathbf{d}_i(t)\| \le d_0$ $\forall t \ge 0$ under the action of the following distributed robust adaptive formation control protocol*

$$\begin{cases} \mathbf{u}_i = \dfrac{1}{\kappa_i}\left(\displaystyle\sum_{j\in\mathcal{N}_i} a_{ij}\dot{\mathbf{v}}_j - \operatorname{diag}\left(\mathbf{K}_{p_i}\right)\boldsymbol{\xi}_i - \operatorname{diag}\left(\mathbf{K}_{v_i}\right)\boldsymbol{\zeta}_i\right) \\ \dot{\mathbf{K}}_{p_i} = -\sigma\left(\mathbf{K}_{p_i} - \mathbf{1}_3\right) + \Gamma_p \operatorname{diag}\left(\boldsymbol{\xi}_i\right)\boldsymbol{\xi}_i \\ \dot{\mathbf{K}}_{v_i} = -\sigma\left(\mathbf{K}_{v_i} - \mathbf{1}_3\right) + \Gamma_v \operatorname{diag}\left(\boldsymbol{\zeta}_i\right)\boldsymbol{\zeta}_i \end{cases} \tag{17}$$

$\forall i \in \{1, \dots, N\}$ where $\kappa_i = \sum_{j\in\mathcal{N}_i} a_{ij}$, $\sigma > 0$, $\Gamma_p > 0$ and $\Gamma_v > 0$. Note that all the initial values of the controller gains $\mathbf{K}_{p_i}$ and $\mathbf{K}_{v_i}$ are greater than or equal to 1.

Proof. By plugging the proposed control protocol (17) into (5), we obtain

$$\dot{\mathbf{v}}_i = \frac{1}{\kappa_i}\left(\sum_{j\in\mathcal{N}_i} a_{ij}\dot{\mathbf{v}}_j - \operatorname{diag}\left(\mathbf{K}_{p_i}\right)\boldsymbol{\xi}_i - \operatorname{diag}\left(\mathbf{K}_{v_i}\right)\boldsymbol{\zeta}_i\right) + \mathbf{d}_i. \tag{18}$$

Multiplying κ_i on both sides of Eq. (18), we get

$$\kappa_i\dot{\mathbf{v}}_i = \Big(\sum_{j\in\mathcal{N}_i} a_{ij}\dot{\mathbf{v}}_j - \text{diag}\left(\mathbf{K}_{p_i}\right)\boldsymbol{\xi}_i - \text{diag}\left(\mathbf{K}_{v_i}\right)\boldsymbol{\zeta}_i\Big) + \hat{\mathbf{d}}_i, \tag{19}$$

where $\hat{\mathbf{d}}_i = \kappa_i\mathbf{d}_i$ and $\|\hat{\mathbf{d}}_i(t)\| \le \kappa_i d_0 = \hat{d}_0\ \forall t \ge 0$. By rearranging Eq. (19) and using the fact that $\kappa_i = \sum_{j\in\mathcal{N}_i} a_{ij}$, we get

$$\sum_{j\in\mathcal{N}_i} a_{ij}(\dot{\mathbf{v}}_i - \dot{\mathbf{v}}_j) = -\text{diag}\left(\mathbf{K}_{p_i}\right)\boldsymbol{\xi}_i - \text{diag}\left(\mathbf{K}_{v_i}\right)\boldsymbol{\zeta}_i + \hat{\mathbf{d}}_i. \tag{20}$$

By differentiating $\boldsymbol{\zeta}_i$ and using $\dot{\boldsymbol{\zeta}}_i = \ddot{\boldsymbol{\xi}}_i$ and $\boldsymbol{\zeta}_i = \dot{\boldsymbol{\xi}}_i$, we derive the formation tracking error dynamics

$$\ddot{\boldsymbol{\xi}}_i = -\text{diag}\left(\mathbf{K}_{p_i}\right)\boldsymbol{\xi}_i - \text{diag}\left(\mathbf{K}_{v_i}\right)\dot{\boldsymbol{\xi}}_i + \hat{\mathbf{d}}_i. \tag{21}$$

Since the closed-loop translational dynamics of each UAV in Eq. (5) are decoupled along the X, Y and Z axes, one-dimensional analysis[1] is reasonably valid. As a result, without loss of generality, we can assume $\xi_i \in \mathbb{R}^1$, $\dot{\xi}_i \in \mathbb{R}^1$, $K_{p_i} \in \mathbb{R}^1$ and $K_{v_i} \in \mathbb{R}^1$ in the remaining part of this proof.

Consider the following Lyapunov function candidate:

$$V = \frac{1}{2}\sum_{i=1}^{N}\xi_i^2 + \sum_{i=1}^{N}\dot{\xi}_i^2 + \frac{1}{4\Gamma_p}\sum_{i=1}^{N}\tilde{K}_{p_i}^2 + \frac{1}{2\Gamma_v}\sum_{i=1}^{N}\tilde{K}_{v_i}^2 \tag{22}$$

where $\tilde{K}_{p_i} \triangleq K_{p_i} - \alpha$, $\tilde{K}_{v_i} \triangleq K_{v_i} - \alpha$ and $\alpha \ge 1$ is a small positive constant. It is not difficult to verify that V is positive definite w.r.t. ξ_i, $\dot{\xi}_i$, $\tilde{K}_{p_i}$ and $\tilde{K}_{v_i}\ \forall i \in \{1,\dots,N\}$ and $V(0) = 0$. The time derivative of V along the trajectories of Eqs. (17) and (21) is

$$\begin{aligned}
\dot{V} &= \sum_{i=1}^{N}\xi_i\dot{\xi}_i + 2\sum_{i=1}^{N}\dot{\xi}_i\ddot{\xi}_i + \frac{1}{2\Gamma_p}\sum_{i=1}^{N}\tilde{K}_{p_i}\dot{\tilde{K}}_{p_i} + \frac{1}{\Gamma_v}\sum_{i=1}^{N}\tilde{K}_{v_i}\dot{\tilde{K}}_{v_i}\\
&= \sum_{i=1}^{N}\Bigg(\xi_i\dot{\xi}_i - 2K_{p_i}\xi_i\dot{\xi}_i - 2K_{v_i}\dot{\xi}_i^2 + 2\dot{\xi}_i\hat{d}_i\\
&\quad + \frac{1}{2\Gamma_p}\tilde{K}_{p_i}\dot{K}_{p_i} + \frac{1}{\Gamma_v}\tilde{K}_{v_i}\dot{K}_{v_i}\Bigg)\\
&\le \sum_{i=1}^{N}\Bigg[\frac{\xi_i^2}{2} + \frac{\dot{\xi}_i^2}{2} - K_{p_i}\xi_i^2 - K_{p_i}\dot{\xi}_i^2 - 2K_{v_i}\dot{\xi}_i^2 + \dot{\xi}_i^2 + \hat{d}_0^2\\
&\quad + \frac{1}{2\Gamma_p}\left(K_{p_i} - \alpha\right)\left(-\sigma(K_{p_i} - 1) + \Gamma_p\xi_i^2\right)\\
&\quad + \frac{1}{\Gamma_v}\left(K_{v_i} - \alpha\right)\left(-\sigma(K_{v_i} - 1) + \Gamma_v\zeta_i^2\right)\Bigg]\\
&= \sum_{i=1}^{N}\Bigg[\left(\frac{1}{2} - \frac{K_{p_i}}{2}\right)\xi_i^2 + \left(\frac{3}{2} - K_{p_i} - K_{v_i}\right)\dot{\xi}_i^2 + \hat{d}_0^2 - \frac{\alpha}{2}\xi_i^2\\
&\quad - \frac{\sigma}{2\Gamma_p}\left(K_{p_i} - \alpha\right)\left(K_{p_i} - 1\right) - \alpha\dot{\xi}_i^2 - \frac{\sigma}{\Gamma_v}\left(K_{v_i} - \alpha\right)\left(K_{v_i} - 1\right)\Bigg]
\end{aligned} \tag{23}$$

where we have used the condition $\|\hat{d}_i(t)\| \le \hat{d}_0\ \forall t \ge 0$ and Lemma 1 to get inequality (23).

Since $K_{p_i}(0) \ge 1$, and when $K_{p_i} = 1$ in (17), $\dot{K}_{p_i} \ge 0$, hence, $K_{p_i}(t) \ge 1\ \forall t \ge 0$. Similarly, since $K_{v_i}(0) \ge 1$, and when $K_{v_i} = 1$ in (17), $\dot{K}_{v_i} \ge 0$, hence, $K_{v_i}(t) \ge 1\ \forall t \ge 0$. Using the fact $K_{p_i}(t) \ge 1$ and $K_{v_i}(t) \ge 1$, (23) can be simplified as

$$\begin{aligned}
\dot{V} \le \sum_{i=1}^{N}\Bigg[&\hat{d}_0^2 - \frac{\alpha}{2}\xi_i^2 - \frac{\sigma}{2\Gamma_p}\left(K_{p_i} - \alpha\right)\left(K_{p_i} - 1\right)\\
&- \alpha\dot{\xi}_i^2 - \frac{\sigma}{\Gamma_v}\left(K_{v_i} - \alpha\right)\left(K_{v_i} - 1\right)\Bigg].
\end{aligned} \tag{24}$$

[1] The interested readers can refer to Ji and Egerstedt (2007).

Upon selecting $0 < \delta \le \alpha - 1$, the inequality condition in (24) can be expressed in a more elegant and manageable form

$$\begin{aligned}
\dot{V} &\le -\delta V + \sum_{i=1}^{N}\Bigg[\frac{(\alpha-1)}{2}\xi_i^2 + (\alpha-1)\dot{\xi}_i^2 + \frac{(\alpha-1)}{4\Gamma_p}\tilde{K}_{p_i}^2\\
&\quad + \frac{(\alpha-1)}{2\Gamma_v}\tilde{K}_{v_i}^2 + \hat{d}_0^2 - \frac{\alpha}{2}\xi_i^2 - \frac{\sigma}{2\Gamma_p}\left(K_{p_i} - \alpha\right)\left(K_{p_i} - 1\right)\\
&\quad - \alpha\dot{\xi}_i^2 - \frac{\sigma}{\Gamma_v}\left(K_{v_i} - \alpha\right)\left(K_{v_i} - 1\right)\Bigg]\\
&\le -\delta V + \sum_{i=1}^{N}\Bigg[\hat{d}_0^2 + \frac{(\alpha-1)}{4\Gamma_p}\tilde{K}_{p_i}^2 + \frac{(\alpha-1)}{2\Gamma_v}\tilde{K}_{v_i}^2\\
&\quad - \frac{\sigma}{2\Gamma_p}\left(K_{p_i} - \alpha\right)\left(K_{p_i} - 1\right) - \frac{\sigma}{\Gamma_v}\left(K_{v_i} - \alpha\right)\left(K_{v_i} - 1\right)\Bigg].
\end{aligned} \tag{25}$$

Using the following assertions:

$$\begin{aligned}
-\frac{\sigma}{2\Gamma_p}\left(K_{p_i} - \alpha\right)\left(K_{p_i} - 1\right) &= -\frac{\sigma}{2\Gamma_p}\tilde{K}_{p_i}\left(\tilde{K}_{p_i} + \alpha - 1\right)\\
&\le -\frac{\sigma}{4\Gamma_p}\tilde{K}_{p_i}^2 + \frac{\sigma}{4\Gamma_p}(\alpha-1)^2
\end{aligned} \tag{26}$$

and

$$\begin{aligned}
-\frac{\sigma}{\Gamma_v}\left(K_{v_i} - \alpha\right)\left(K_{v_i} - 1\right) &= -\frac{\sigma}{\Gamma_v}\tilde{K}_{v_i}\left(\tilde{K}_{v_i} + \alpha - 1\right)\\
&\le -\frac{\sigma}{2\Gamma_v}\tilde{K}_{v_i}^2 + \frac{\sigma}{2\Gamma_v}(\alpha-1)^2,
\end{aligned} \tag{27}$$

we can rewrite the inequality in (25) as

$$\begin{aligned}
\dot{V} \le -\delta V + \sum_{i=1}^{N}\Bigg[&\hat{d}_0^2 + \frac{(\alpha-1-\sigma)}{4\Gamma_p}\tilde{K}_{p_i}^2 + \frac{(\alpha-1-\sigma)}{2\Gamma_v}\tilde{K}_{v_i}^2\\
&+ \frac{\sigma}{4\Gamma_p}(\alpha-1)^2 + \frac{\sigma}{2\Gamma_v}(\alpha-1)^2\Bigg].
\end{aligned} \tag{28}$$

Finally, by choosing $\sigma \ge \alpha - 1$, we can get that

$$\dot{V} \le -\delta V + \sum_{i=1}^{N}\left[\hat{d}_0^2 + \frac{\sigma}{4\Gamma_p}(\alpha-1)^2 + \frac{\sigma}{2\Gamma_v}(\alpha-1)^2\right]. \tag{29}$$

Since the terms in the right-hand side of the above inequality are all finite and deterministic, applying Lemma 2, we can ensure the $V(\cdot)$ function is bounded. This, in turn, guarantees the ultimate boundedness of the formation error $\boldsymbol{\xi}_i$, velocity error $\boldsymbol{\zeta}_i$, and the controller gains $\mathbf{K}_{p_i}$ and $\mathbf{K}_{v_i}$ when the multi-UAV system is subjected to bounded exogenous disturbances $\|\mathbf{d}_i\| \le d_0$. This completes the proof. ■

Remark 2. The proposed distributed robust adaptive formation control protocol in Eq. (17) provides a simple, yet effective solution to preserve formation tracking stability of the multi-UAV system in the presence of unknown bounded exogenous disturbances. By utilising the σ-modification technique, we ensure the formation error $\boldsymbol{\xi}_i$, the velocity error $\boldsymbol{\zeta}_i$, the controller gains $\mathbf{K}_{p_i}$ and $\mathbf{K}_{v_i}$ remain bounded. Compared to existing techniques (e.g. Baldi and Frasca (2019), Cardona et al. (2021), Dogan et al. (2019), Liu et al. (2020), Wang et al. (2022) and Xuan-Mung and Hong (2019)), the proposed methodology does not require any reference model, disturbance filter/observer, or any prior knowledge of the exogenous disturbances.

In a cooperative payload transportation mission, one end of the cable/string is attached to the payload, and the other end is attached close to the battery position on each UAV, which is close to the Centre of Mass. As a result, we assume that the tensile disturbances caused by the cables/strings carrying the suspended payload have negligible effects on the rotational dynamics of each quadcopter UAV. Instead, they can be captured by the term $\mathbf{d}_i$ included in the closed-loop translational dynamics in Eq. (5).

According to Theorem 1, the multi-UAV system achieves the desired formation and synchronises its motions to keep tracking the

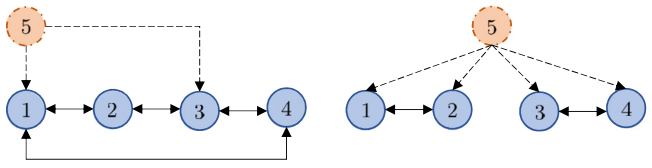

(a) Topology 1. (b) Topology 2.

Fig. 3. Interaction topologies. The virtual leader/target is labelled as 5. Note that both interaction topologies satisfy Assumption 1. (a) Topology 1 is used for the Matlab simulation case study; (b) Topology 2 is used for the real-time flight experiments.

assigned virtual leader/target in the presence of unknown bounded exogenous disturbances $\mathbf{d}_i$. Therefore, the cooperative payload transportation problem by multi-UAV systems can be solved by implementing the proposed distributed robust adaptive formation control protocol in Theorem 1. It should be highlighted that the proposed robust adaptive formation control methodology reduces the overall complexity of the solution to the cooperative payload transportation problem. This is because it does not require prior knowledge about the suspended payload, nor does it require any additional sensors to measure state information for the suspended payload.

4. Matlab simulation case study

In the Matlab simulation case study, we address a two-dimensional formation tracking problem for four networked agents whose translational dynamics are approximated by double integrator dynamics as in Eq. (5), where each agent is subjected to bounded exogenous disturbances. Fig. 3(a) depicts the interaction topology between each agent and the virtual leader/target. Furthermore, the formation configuration is specified so that four networked agents form a two-dimensional diamond shape formation, with the centre being the virtual leader/target. The exogenous disturbances injected on each agent are $\mathbf{d}_1 = [0.5\sin t, 0.6\cos 2t]^\top$, $\mathbf{d}_2 = [0.9\cos 4t, 0.2\sin 3t]^\top$, $\mathbf{d}_3 = [0.1\sin 2t, 0.3\sin 3t]^\top$, $\mathbf{d}_4 = [0.4\cos 4t, 0.7\cos t]^\top$, and the motion reference of the virtual leader/target as $\mathbf{a}_{\text{ref}} = [e^{-0.1t}, 0]^\top$. We set $\mathbf{K}_{p_i}(0) = 2$ and $\mathbf{K}_{v_i}(0) = 2 \quad \forall i \in \{1, \dots, 4\}$, $\Gamma_p = 0.05$, $\Gamma_v = 0.05$, and $\sigma = 1$.

To indicate the robustness of the proposed formation controller against the exogenous disturbances, a benchmark adaptive formation controller was selected from a recent article (Hu, Bhowmick, Jang et al., 2021) for comparison, where the adaptive law is formulated as follows

$$\begin{cases} \dot{\mathbf{K}}_{p_i} = \operatorname{diag}\left(\boldsymbol{\xi}_i\right) \operatorname{diag}\left(\Gamma_p\right) \boldsymbol{\xi}_i \\ \dot{\mathbf{K}}_{v_i} = \operatorname{diag}\left(\boldsymbol{\zeta}_i\right) \operatorname{diag}\left(\Gamma_v\right) \boldsymbol{\zeta}_i \end{cases} \tag{30}$$

$\forall i \in \{1, \dots, N\}$ where $\boldsymbol{\Gamma}_p > 0$, $\boldsymbol{\Gamma}_v > 0$, $\mathbf{K}_{p_i}(0) \geq 0$ and $\mathbf{K}_{v_i}(0) \geq 0$.

Remark 3. Because of the bounded exogenous disturbances $\mathbf{d}_i$ in Eq. (5), the formation error $\boldsymbol{\xi}_i$ and velocity error $\boldsymbol{\zeta}_i$ will not converge to zero, but to a small neighbourhood close to zero. Therefore, the controller gains $\mathbf{K}_{p_i}$ and $\mathbf{K}_{v_i}$ in Eq. (30) are subject to the parameter drift phenomenon (Ioannou & Sun, 1995).

Fig. 4 compares the formation errors and controller gains $\mathbf{K}_p$ and $\mathbf{K}_v$ between the proposed robust adaptive formation controller in Fig. 4(a) and the benchmark adaptive formation controller from article (Hu, Bhowmick, Jang et al., 2021) in Fig. 4(b). The controller gains $\mathbf{K}_p$ and $\mathbf{K}_v$ are bounded in Fig. 4(a) but they drift and eventually diverge to infinity in Fig. 4(b). As a result of the parameter drift phenomenon, the formation errors $\boldsymbol{\xi}_i(t)$ also diverge to infinity eventually in Fig. 4(b). The results demonstrate that the proposed robust adaptive formation controller in Eq. (17) solves the parameter drift phenomenon. In addition, the formation errors and controller gains are guaranteed to be bounded when networked agents travel in a formation and synchronise their motions with the virtual leader/target in the presence of bounded exogenous disturbances.

Remark 4. According to the proposed robust adaptive formation control protocol in Eq. (17) and by choosing $\sigma > 0$, the formation errors and controller gains are ensured to converge to and remain within a bounded interval. In addition, the parameter σ determines the convergence rate for the controller gains and the range of the bounded interval of the formation errors. By increasing the value of σ, the controller gains converge to a bounded interval faster, but the bounded interval of the formation errors also becomes larger. Therefore, the selection of σ should be carefully considered with respect to the trade-off between the convergence rate of the controller gains and the range of the bounded interval for the formation errors.

5. Experimental validation results

To validate the feasibility and performance of the proposed robust adaptive formation control methodology, we implemented it on a team of networked Crazyflie 2.1 nano quadcopters and conducted two real-time flight experiments. In this section, we will first introduce the Crazyflie 2.1 nano quadcopter and the setup of the flight experiment. We will then describe the scenarios of two real-time flight experiments. Finally, we will present and discuss the experimental results. A recorded video clip of the two real-time flight experiments can be found in the Supplementary Material and at https://youtu.be/6ZlPhaR3was.

5.1. Experimental setup

Fig. 5 presents the Crazyflie 2.1 nano quadcopter with expansion decks, including the Flow deck v2 and the Loco Positioning deck. Crazyflie is a small size (the diagonal length is 92 mm from motor to motor) and lightweight (about 25 g) quadcopter, developed as an open-source flying platform by Bitcraze (0000). According to Bitcraze (0000), the maximum recommended payload weight is only 15 g. Furthermore, the Loco Positioning system (LPS) provides the absolute position of each Crazyflie nano quadcopter (Bitcraze, 0000). Note that the positioning accuracy of the LPS is within 0.1 m.

Fig. 6 describes the hardware control configuration of the real-time flight experiments. The attitude and attitude rate PID controllers in the inner control loop are embedded onboard each Crazyflie, while the proposed distributed robust adaptive formation controller in the outer control loop is implemented in a base station PC. The estimated states of each quadcopter are transmitted to the base station PC, and the control commands are generated through the base station PC and sent to each quadcopter via Crazyradio dongles (Bitcraze, 0000). However, if each quadcopter can directly measure the relative positions of its neighbours or share its states with its neighbours via Bluetooth or Wi-fi, the base station PC can be removed, and the proposed robust adaptive formation controller can be directly implemented on each quadcopter because the proposed robust adaptive formation control protocol in Eq. (17) is completely distributed, requiring only neighbouring states.

Remark 5. The proposed distributed robust adaptive formation control law in (17) can be easily implemented on the microprocessor on each quadcopter UAV since it only relies on addition and multiplication operations. Moreover, compared to Lee (2018), Michael et al. (2011) and Tartaglione et al. (2017), the proposed methodology can be easily applied to a large group of agents/UAVs without imposing a heavy computational burden due to its distributed nature.

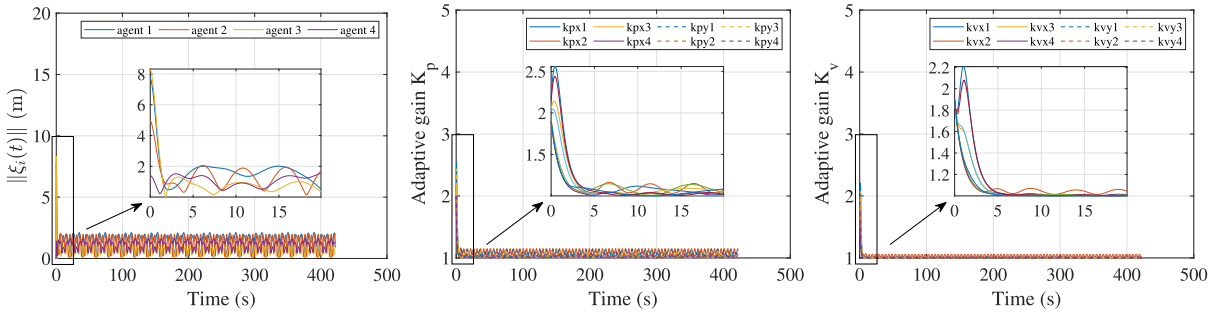

(a) The proposed robust adaptive formation controller in this paper.

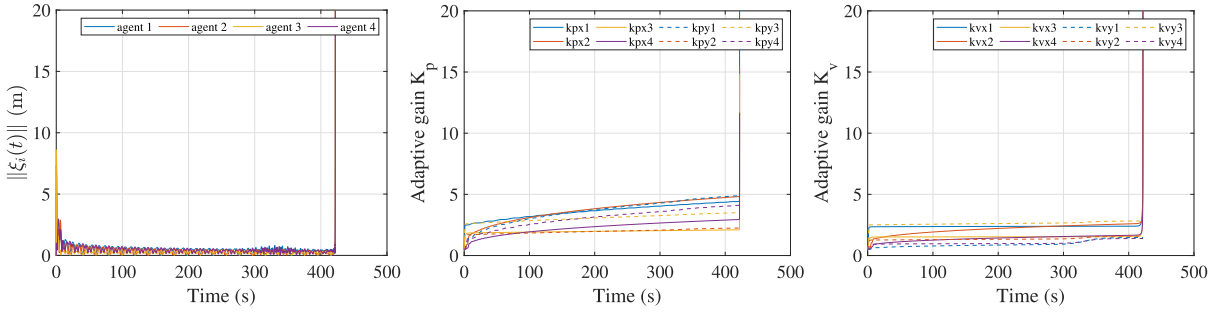

(b) The benchmark adaptive formation controller from article (Hu, Bhowmick, Jang et al., 2021).

Fig. 4. Comparison of the 2-norm of the formation error $\|\xi_i(t)\|$ of each agent, controller gains $\mathbf{K}_p$ and $\mathbf{K}_v$ when networked agents are subjected to bounded exogenous disturbances.

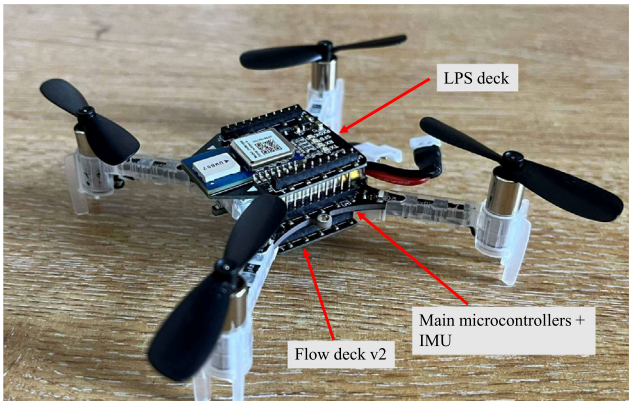

Fig. 5. A Crazyflie 2.1 nano quadcopter with expansion decks.

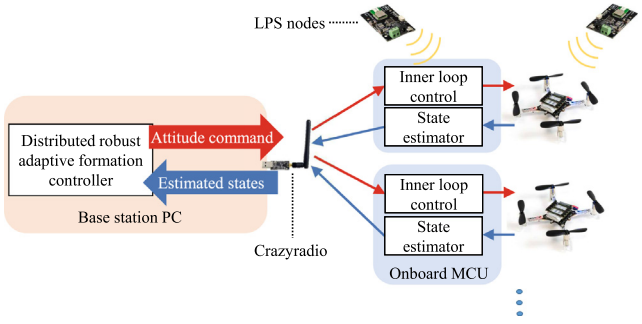

Fig. 6. The hardware control configuration for the quadcopter flight experiments. Crazyradios are used to collect estimated states (i.e. positions, velocities and accelerations) from all Crazyflie quadcopters and broadcast control signals to them. A coordinate reference is provided by a set of eight LPS nodes, which are part of the Loco Positioning system.

5.2. Experiment 1: Formation tracking flight mission

In experiment 1, a team of four networked Crazyflie nano quadcopters is used to perform an autonomous formation tracking flight mission. We aim to implement the proposed distributed robust adaptive formation controller on each Crazyflie quadcopter and examine the formation tracking performance. Fig. 3(b) describes the interaction topology between each quadcopter and the virtual leader/target. Furthermore, the formation configuration is specified so that four networked quadcopter UAVs form a diamond shape formation, with the centre being the virtual leader/target.

In the experiment, we set $\mathbf{K}_{p_i}(0) = 1.5$ and $\mathbf{K}_{v_i}(0) = 1.2 \quad \forall i \in \{1, \dots, 4\}$, $\Gamma_p = 0.1$, $\Gamma_v = 0.05$, and $\sigma = 0.1$. The initial position of each quadcopter is $\mathbf{p}_1(0) = [-1.2, -1.9, 0]^\top$, $\mathbf{p}_2(0) = [-1.8, -1.6, 0]^\top$, $\mathbf{p}_3(0) = [-2.1, -2.8, 0]^\top$, and $\mathbf{p}_4(0) = [-2.5, -2.4, 0]^\top$. The initial position of the virtual leader/target is $\mathbf{p}_5(0) = [-2, -2, 1]^\top$ and its velocity is chosen as

$$
\begin{aligned}
v_{x_5}(t) &= \begin{cases} 0\,\text{m/s}, & 0\,\text{s} \le t \le 5\,\text{s}, \\ 0.3\,\text{m/s}, & 5\,\text{s} < t \le 15\,\text{s}, \\ 0\,\text{m/s}, & 15\,\text{s} < t \le 25\,\text{s}, \end{cases} \\
v_{y_5}(t) &= \begin{cases} 0\,\text{m/s}, & 0\,\text{s} \le t \le 15\,\text{s}, \\ 0.3\,\text{m/s}, & 15\,\text{s} < t \le 25\,\text{s}, \end{cases} \\
v_{z_5}(t) &= 0\,\text{m/s}, \quad 0\,\text{s} \le t \le 25\,\text{s}.
\end{aligned} \tag{31}
$$

Fig. 7 presents the trajectories of all quadcopters in the X–Y plane. A team of four quadcopters first formed a diamond shape formation, as shown in Fig. 7(b). Then, they maintained the diamond shape formation and synchronised their motions with the virtual leader/target (refer to Fig. 7(c) and (d)). The formation errors and controller gains $\mathbf{K}_p$ and $\mathbf{K}_v$ of the robust adaptive formation controller are shown in Fig. 8. The formation error of each quadcopter converges and remains close to zero, and all controller gains $\mathbf{K}_p$ and $\mathbf{K}_v$ are bounded. Fig. 9 shows the velocities in the X, Y and Z directions of all quadcopters and the virtual leader/target, in which all quadcopters track the velocity

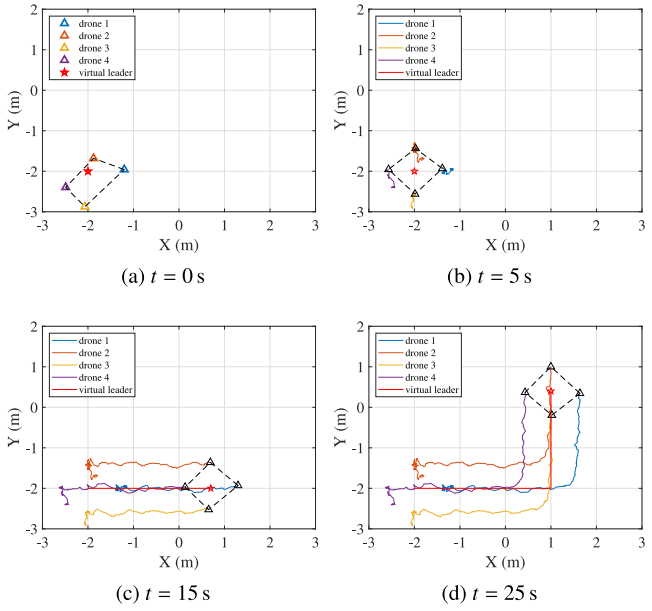

Fig. 7. Trajectories of all quadcopters in the X–Y plane at time instants $t = 0$ s, $t = 5$ s, $t = 15$ s and $t = 25$ s of Experiment 1. The black dashed lines represent the formations of all quadcopters. The triangles and the red stars mark the positions of each quadcopter and the virtual leader/target at each time instant, respectively. (a) At $t = 0$ s, the quadcopters started from random positions; (b) At $t = 5$ s, the quadcopters achieved the prescribed diamond shape formation; (c) At $t = 15$ s, the quadcopters maintained the diamond shape formation and synchronised their motions with the virtual leader/target; (d) At $t = 25$ s, mission complete. (For interpretation of the references to colour in this figure legend, the reader is referred to the web version of this article.)

of the virtual leader/target in a few seconds. The results demonstrate that four networked quadcopter UAVs successfully accomplished the formation tracking flight mission by implementing the proposed robust adaptive formation control methodology.

5.3. Experiment 2: Cooperative payload transportation flight mission

Experiment 2 aims to demonstrate a cooperative payload transportation flight mission in 3D space by implementing the proposed distributed robust adaptive formation controller on networked quadcopter UAVs. In the experiment, four networked Crazyflie nano quadcopters are deployed to transport a suspended payload. The goal is for the four networked quadcopter UAVs to achieve the desired formation and synchronise their motions with the virtual leader/target to cooperatively transport the suspended payload to its final destination. Note that in this experiment, the virtual leader has a velocity in X, Y and Z directions simultaneously, resulting in a 3D diagonal trajectory. Fig. 3(b) describes the interaction topology between each quadcopter and the virtual leader/target. Furthermore, the formation configuration is specified so that four networked quadcopter UAVs form a square formation, with the centre being the virtual leader/target. Cables/strings are attached close to the battery position on each quadcopter UAV, which is close to the Centre of Mass. Therefore, we may assume that the cable-suspended payload has almost no effect on the rotational dynamics of each quadcopter UAV. However, this is not a restrictive assumption since the Centre of Mass of a small quadcopter, such as the Crazyflie 2.1 nano quadcopter, usually coincides with the battery position.

In the experiment, we set $\mathbf{K}_{p_i}(0) = 1.5$ and $\mathbf{K}_{v_i}(0) = 1.2 \quad \forall i \in \{1, \dots, 4\}$, $\Gamma_p = 0.1$, $\Gamma_v = 0.05$ and $\sigma = 0.1$. The initial position of each quadcopter is $\mathbf{p}_1(0) = [0.35, 0.31, 0]^\top$, $\mathbf{p}_2(0) = [-0.36, 0.28, 0]^\top$, $\mathbf{p}_3(0) = [0.35, -0.43, 0]^\top$, and $\mathbf{p}_4(0) = [-0.45, -0.41, 0]^\top$. The initial position of the virtual leader/target is $\mathbf{p}_5(0) = [0, 0, 1]^\top$ and its velocity is chosen as

$$
\begin{aligned}
v_{x_5}(t) &= \begin{cases} 0\,\text{m/s}, & 0\,\text{s} \le t \le 5\,\text{s}, \\ 0.2\,\text{m/s}, & 5\,\text{s} < t \le 15\,\text{s}, \end{cases} \\
v_{y_5}(t) &= \begin{cases} 0\,\text{m/s}, & 0\,\text{s} \le t \le 5\,\text{s}, \\ 0.1\,\text{m/s}, & 5\,\text{s} < t \le 15\,\text{s}, \end{cases} \\
v_{z_5}(t) &= \begin{cases} 0\,\text{m/s}, & 0\,\text{s} \le t \le 5\,\text{s}, \\ 0.05\,\text{m/s}, & 5\,\text{s} < t \le 15\,\text{s}, \end{cases}
\end{aligned} \tag{32}
$$

resulting in a 3D diagonal trajectory.

Fig. 10 shows the trajectories of all quadcopters in 3D space. Fig. 11 presents the snapshots of the cooperative payload transportation flight experiment. Four networked quadcopter UAVs achieved the desired square formation while cooperatively lifting the suspended payload within the first few seconds, as shown in Fig. 11(b). Then, they transported the suspended payload by maintaining the prescribed square formation and tracking the 3D diagonal trajectory of the virtual leader/target. Finally, as shown in Fig. 11(c), they successfully delivered the suspended payload to its final destination. The formation errors and controller gains $\mathbf{K}_p$ and $\mathbf{K}_v$ of the robust adaptive formation controller are shown in Fig. 12. When networked quadcopter UAVs fly in the desired square formation and carry a suspended payload, the formation error of each quadcopter converges and remains close to zero, and all controller gains $\mathbf{K}_p$ and $\mathbf{K}_v$ are bounded. Fig. 13 shows the velocities in the X, Y and Z directions of all quadcopters and the virtual leader/target, in which all quadcopters synchronise their motions with the virtual leader/target while transporting a suspended payload. The results demonstrate that four networked quadcopter

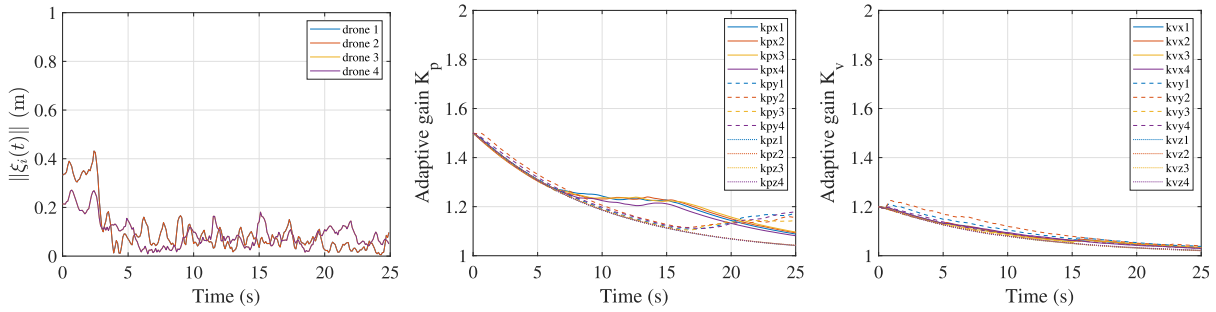

(a) Formation errors. (b) Adaptive gains $\mathbf{K}_p$. (c) Adaptive gains $\mathbf{K}_v$.

Fig. 8. Formation errors and controller gains $\mathbf{K}_p$ and $\mathbf{K}_v$ of Experiment 1. (a) The 2-norm of the formation error $\|\xi_i(t)\|$ of each quadcopter. Note that the formation error does not converge to exactly zero as the positioning accuracy of the LPS is within 0.1 m; (b) The controller gains $\mathbf{K}_p$ of the robust adaptive formation controller are bounded; (c) The controller gains $\mathbf{K}_v$ of the robust adaptive formation controller are bounded.

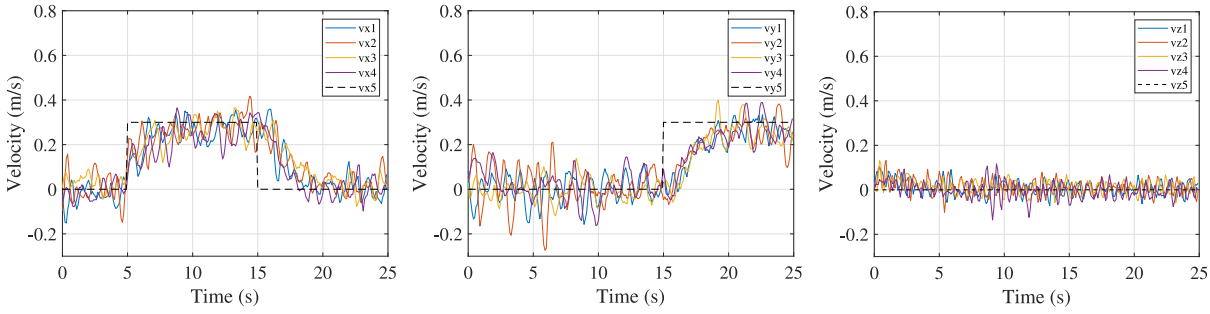

(a) Velocity in the X-direction. (b) Velocity in the Y-direction. (c) Velocity in the Z-direction.

Fig. 9. Velocities of all quadcopters and the virtual leader/target of Experiment 1. The black dashed lines represent the velocity of the virtual leader/target. Note that the velocities of all quadcopters are estimated via the onboard estimators at each time instant.

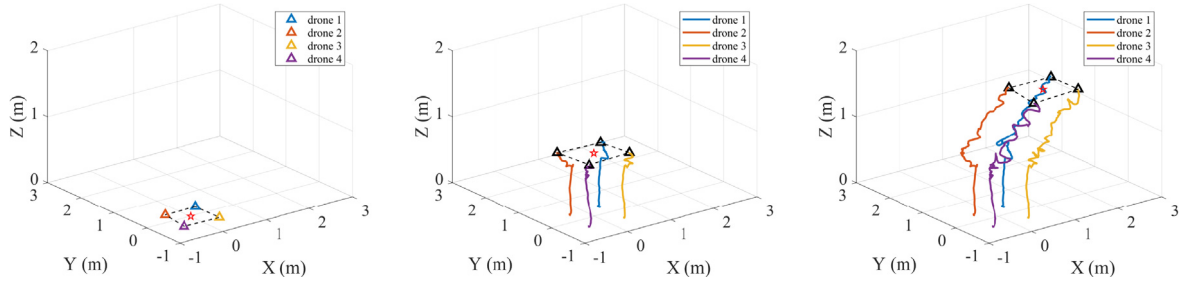

(a) $t = 0$ s (b) $t = 5$ s (c) $t = 15$ s

Fig. 10. Trajectories of all quadcopters in 3D space at time instants $t = 0$ s, $t = 5$ s and $t = 15$ s of Experiment 2. The black dashed lines represent the formations of the quadcopters. The triangles and the red stars mark the positions of each quadcopter and the virtual leader/target at each time instant, respectively. All quadcopters followed the motion of the virtual leader/target, which is a 3D diagonal trajectory. (For interpretation of the references to colour in this figure legend, the reader is referred to the web version of this article.)

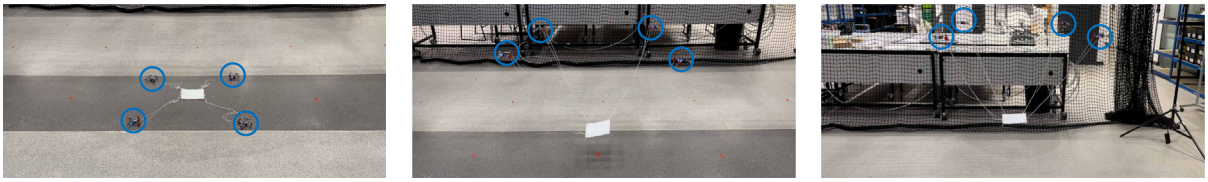

(a) $t = 0$ s (b) $t = 5$ s (c) $t = 15$ s

Fig. 11. Snapshots of Experiment 2 at time instants $t = 0$ s, $t = 5$ s and $t = 15$ s. The blue circles in the snapshots mark the four quadcopters. (a) At $t = 0$ s, the quadcopters started from random positions; (b) At $t = 5$ s, the quadcopters achieved the desired square formation while cooperatively lifting the suspended payload; (c) At $t = 15$ s, all quadcopters reached the final positions, and the suspended payload was also delivered to its final destination, mission complete. (For interpretation of the references to colour in this figure legend, the reader is referred to the web version of this article.)

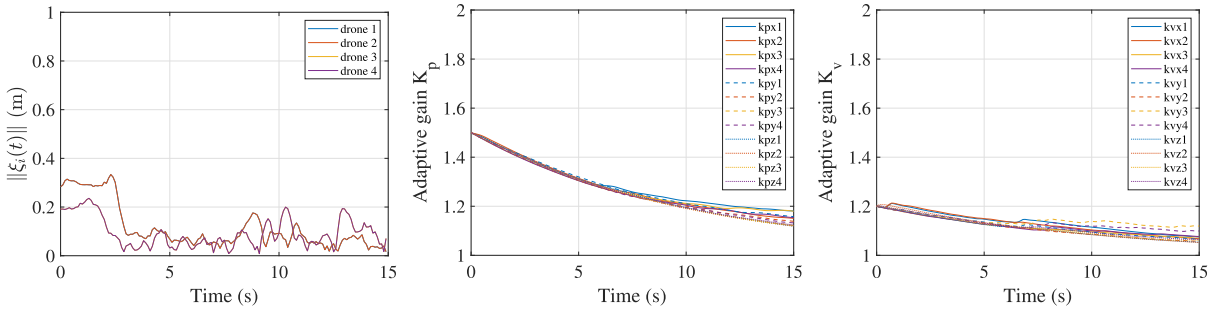

(a) Formation errors. (b) Adaptive gains $\mathbf{K}_p$. (c) Adaptive gains $\mathbf{K}_v$.

Fig. 12. Formation errors and controller gains $\mathbf{K}_p$ and $\mathbf{K}_v$ of Experiment 2. (a) The 2-norm of the formation error $\|\xi_i(t)\|$ of each quadcopter. Note that the formation error does not converge to exactly zero as the positioning accuracy of the LPS is within 0.1 m; (b) The controller gains $\mathbf{K}_p$ of the robust adaptive formation controller are bounded; (c) The controller gains $\mathbf{K}_v$ of the robust adaptive formation controller are bounded.

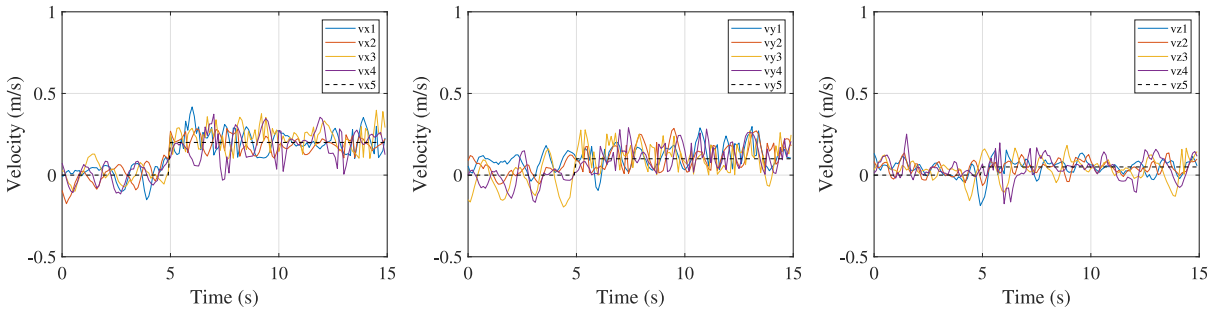

(a) Velocity in the X-direction. (b) Velocity in the Y-direction. (c) Velocity in the Z-direction.

Fig. 13. Velocities of all quadcopters and the virtual leader/target of Experiment 2. The black dashed lines represent the velocity of the virtual leader/target. Note that the velocities of all quadcopters are estimated via the onboard estimators at each time instant.

UAVs successfully accomplished the cooperative payload transportation flight mission by implementing the proposed robust adaptive formation control methodology.

6. Conclusions

This paper proposes a new robust adaptive formation control methodology for networked UAVs subject to bounded exogenous disturbances, which finds potential applications in cooperative payload transportation missions. The proposed methodology exploits the σ-modification approach to theoretically establish the ultimate boundedness of the formation tracking error dynamics and controller gains when networked UAVs fly in the presence of bounded exogenous disturbances. The feasibility and effectiveness of the new formation control scheme have been demonstrated through Matlab simulation case studies and real-time indoor flight experiments on a multi-UAV system (using Crazyflie 2.1 nano quadcopters Bitcraze, 0000). The experimental results also show that the proposed scheme has been successfully implemented to perform a cooperative payload transportation flight mission. In future, Negative-imaginary theory (Bhowmick, Ganguly, & Sen, 2022; Lanzon & Bhowmick, 2023; Lanzon & Chen, 2017; Lanzon & Petersen, 2008) may be explored to develop a state-of-the-art robust cooperative control scheme for networked UAVs, facilitating fault-tolerance and obstacle-avoidance features. The proposed scheme may also be extended to address the collision avoidance problem between adjacent UAVs and the obstacle avoidance problem using a Decentralised Artificial Potential Field method (Tnunay, Li, Wang, & Ding, 2017).

Declaration of competing interest

The authors declare that they have no known competing financial interests or personal relationships that could have appeared to influence the work reported in this paper.

Acknowledgements

The authors would like to express their sincere thanks and gratitude to the anonymous reviewers and the concerned Associate Editor for giving their valuable feedback and constructive suggestions that helped us to improve the quality and clarity of the paper.

This work was supported by the Engineering and Physical Sciences Research Council (EPSRC), UK [grant number EP/R008876/1] and by the Science and Engineering Research Board (SERB), DST, India [grant number SRG/2022/000892]. All research data supporting this publication are directly available within this publication. For the purpose of open access, the authors have applied a Creative Commons Attribution (CC BY) licence to any Author Accepted Manuscript version arising.

Appendix A. Supplementary data

Supplementary material related to this article can be found online at https://doi.org/10.1016/j.conengprac.2023.105608.

References

Amazon prime air. (2016). https://www.amazon.com/b?node=8037720011.

Baldi, S., & Frasca, P. (2019). Adaptive synchronization of unknown heterogeneous agents: An adaptive virtual model reference approach. *Journal of the Franklin Institute*, *356*(2), 935–955.

Bernstein, D. S. (2009). *Matrix mathematics : theory, facts, and formulas*. Princeton, N.J: Princeton University Press, Princeton.

Bhowmick, P., Ganguly, A., & Sen, S. (2022). A new consensus-based formation tracking scheme for a class of robotic systems using negative imaginary property. *IFAC-PapersOnLine*, *55*(1), 685–690.

Bitcraze Crazyflie 2.1 nano quadcopter. URL https://www.bitcraze.io/products/crazyflie-2-1/.

Cardona, G. A., Arevalo-Castiblanco, M., Tellez-Castro, D., Calderon, J., & Mojica-Nava, E. (2021). Robust adaptive synchronization of interconnected heterogeneous quadrotors transporting a cable-suspended load. In *Proceedings of the IEEE international conference on robotics and automation* (pp. 31–37). Xi'an, China: IEEE.

Chen, Z., Zhang, B., Stojanovic, V., Zhang, Y., & Zhang, Z. (2020). Event-based fuzzy control for T-S fuzzy networked systems with various data missing. *Neurocomputing*, *417*, 322–332.

Ding, Z. (2013). *IET control engineering series: Vol. 84, Nonlinear and adaptive control systems*. London: The Institution of Engineering and Technology.

Dogan, K. M., Gruenwald, B. C., Yucelen, T., Muse, J. A., & Butcher, E. A. (2019). Distributed adaptive control and stability verification for linear multiagent systems with heterogeneous actuator dynamics and system uncertainties. *International Journal of Control*, *92*(11), 2620–2638.

Dong, X., Yu, B., Shi, Z., & Zhong, Y. (2015). Time-varying formation control for unmanned aerial vehicles: theories and applications. *IEEE Transactions on Control Systems Technology*, *23*(1), 340–348.

Dong, X., Zhou, Y., Ren, Z., & Zhong, Y. (2016). Time-varying formation control for unmanned aerial vehicles with switching interaction topologies. *Control Engineering Practice*, *46*, 26–36.

Guo, K., Jia, J., Yu, X., Guo, L., & Xie, L. (2020). Multiple observers based anti-disturbance control for a quadrotor UAV against payload and wind disturbances. *Control Engineering Practice*, *102*, Article 104560.

Hu, J., Bhowmick, P., Jang, I., Arvin, F., & Lanzon, A. (2021). A decentralized cluster formation containment framework for multirobot systems. *IEEE Transactions on Robotics*, *37*(6), 1936–1955.

Hu, J., Bhowmick, P., & Lanzon, A. (2020). Distributed adaptive time-varying group formation tracking for multiagent systems with multiple leaders on directed graphs. *IEEE Transactions on Control of Network Systems*, *7*(1), 140–150.

Hu, J., Bhowmick, P., & Lanzon, A. (2021). Group coordinated control of networked mobile robots with applications to object transportation. *IEEE Transactions on Vehicular Technology*, *70*(8), 8269–8274.

Hu, J., & Lanzon, A. (2018). An innovative tri-rotor drone and associated distributed aerial drone swarm control. *Robotics and Autonomous Systems*, *103*, 162–174.

Ioannou, P. A., & Sun, J. (1995). *Robust adaptive control*. Prentice-Hall, Inc..

Ji, M., & Egerstedt, M. (2007). Distributed coordination control of multiagent systems while preserving connectedness. *IEEE Transactions on Robotics*, *23*(4), 693–703.

Kendoul, F. (2009). Nonlinear hierarchical flight controller for unmanned rotorcraft: design, stability, and experiments. *Journal of Guidance, Control, and Dynamics*, *32*(6), 1954–1958.

Klausen, K., Meissen, C., Fossen, T. I., Arcak, M., & Johansen, T. A. (2020). Cooperative control for multirotors transporting an unknown suspended load under environmental disturbances. *IEEE Transactions on Control Systems Technology*, *28*(2), 653–660.

Lanzon, A., & Bhowmick, P. (2023). Characterisation of input-output negative imaginary systems in a dissipative framework. *IEEE Transactions on Automatic Control*, *68*(2), 959–974.

Lanzon, A., & Chen, H.-J. (2017). Feedback stability of negative imaginary systems. *IEEE Transactions on Automatic Control*, *62*(11), 5620–5633.

Lanzon, A., & Petersen, I. R. (2008). Stability robustness of a feedback interconnection of systems with negative imaginary frequency response. *IEEE Transactions on Automatic Control*, *53*(4), 1042–1046.

Lee, T. (2018). Geometric control of quadrotor UAVs transporting a cable-suspended rigid body. *IEEE Transactions on Control Systems Technology*, *26*(1), 255–264.

Lindsey, Q., Mellinger, D., & Kumar, V. (2012). Construction with quadrotor teams. *Autonomous Robots*, *33*(3), 323–336.

Liu, H., Ma, T., Lewis, F. L., & Wan, Y. (2020). Robust formation control for multiple quadrotors with nonlinearities and disturbances. *IEEE Transactions on Cybernetics*, *50*(4), 1362–1371.

Marina, H. G. d., & Smeur, E. (2019). Flexible collaborative transportation by a team of rotorcraft. In *Proceedings of the IEEE international conference on robotics and automation* (pp. 1074–1080). IEEE.

Maza, I., Kondak, K., Bernard, M., & Ollero, A. (2010). Multi-UAV cooperation and control for load transportation and deployment. *Journal of Intelligent and Robotic Systems*, *57*, 417–449.

Meng, Z., Ren, W., & You, Z. (2010). Distributed finite-time attitude containment control for multiple rigid bodies. *Automatica*, *46*(12), 2092–2099.

Michael, N., Fink, J., & Kumar, V. (2011). Cooperative manipulation and transportation with aerial robots. *Autonomous Robots*, *30*(1), 73–86.

Mohammadi, K., Sirouspour, S., & Grivani, A. (2020). Control of multiple quad-copters with a cable-suspended payload subject to disturbances. *IEEE/ASME Transactions on Mechatronics*, *25*(4), 1709–1718.

Ren, W., Beard, R. W., & Atkins, E. M. (2007). Information consensus in multivehicle cooperative control. *IEEE Control Systems Magazine*, *27*(2), 71–82.

Su, Y.-H., & Lanzon, A. (2022). Formation-containment tracking and scaling for multiple quadcopters with an application to choke-point navigation. In *Proceedings of the IEEE international conference on robotics and automation* (pp. 4908–4914). IEEE.

Tartaglione, G., D'Amato, E., Ariola, M., Rossi, P. S., & Johansen, T. A. (2017). Model predictive control for a multi-body slung-load system. *Robotics and Autonomous Systems*, *92*, 1–11.

Tnunay, H., Li, Z., Wang, C., & Ding, Z. (2017). Distributed collision-free coverage control of mobile robots with consensus-based approach. In *Proceedings of the IEEE international conference on control and automation* (pp. 678–683). IEEE.

Toksoz, M. A., Oguz, S., & Gazi, V. (2019). Decentralized formation control of a swarm of quadrotor helicopters. In *Proceedings of the 15th IEEE international conference on control and automation* (pp. 1006–1013). Edinburgh, Scotland.

Turpin, M., Michael, N., & Kumar, V. (2012). Decentralized formation control with variable shapes for aerial robots. In *Proceedings of the IEEE international conference on robotics and automation* (pp. 23–30). IEEE.

Villa, D. K. D., Brandao, A. S., & Sarcinelli-Filho, M. (2019). Rod-shaped payload transportation using multiple quadrotors. In *Proceedings of the international conference on unmanned aircraft systems* (pp. 1036–1040). Atlanta, GA, USA: IEEE.

Wang, J., Bi, C., Wang, D., Kuang, Q., & Wang, C. (2022). Finite-time distributed event-triggered formation control for quadrotor UAVs with experimentation. *ISA Transactions*, *126*, 585–596.

Wang, G., Yang, W., Zhao, N., Ji, Y., Shen, Y., Xu, H., et al. (2020). Distributed consensus control of multiple UAVs in a constrained environment. In *Proceedings of the IEEE international conference on robotics and automation* (pp. 3234–3240). Paris, France.

Xuan-Mung, N., & Hong, S. K. (2019). Robust adaptive formation control of quadcopters based on a leader–follower approach. *International Journal of Advanced Robotic Systems*, *16*(4).

Zhou, L., Tao, H., Paszke, W., Stojanovic, V., & Yang, H. (2020). PD-type iterative learning control for uncertain spatially interconnected systems. *Mathematics*, *8*(9), 1528.